Environmental Science & Technology

pubs.acs.org/est

Article

Mechanistic Investigation of Haloacetic Acid Reduction Using Carbon-Ti_4O_7 Composite Reactive Electrochemical Membranes

Soroush Almassi, Pamela Rose V. Samonte, Zhao Li, Wenqing Xu, and Brian P. Chaplin*

Cite This: *Environ. Sci. Technol.* 2020, 54, 1982−1991

Read Online

ACCESS | Metrics & More | Article Recommendations | Supporting Information

ABSTRACT: Carbon-Ti_4O_7 composite reactive electrochemical membranes (REMs) were studied for adsorption and electrochemical reduction of haloacetic acids (HAAs). Powder activated carbon (PAC) or multiwalled carbon nanotubes (MWCNTs) were used in these composites. Results from flow-through adsorption experiments with dibromoacetic acid (DBAA) as a model HAA were interpreted with a transport model. It was estimated that ∼46% of C in the MWCNT-REM and ∼10% of C in the PAC-REM participated in adsorption reactions. Electrochemical reduction of 1 mg L^{-1} DBAA in 10 mM KH_2PO_4/K_2HPO_4 at −1.5 V/SHE (hydraulic residence time, ∼11 s) resulted in 73, 94, and 96% DBAA reduction for Ti_4O_7, PAC-Ti_4O_7, and MWCNT-Ti_4O_7 REMs, respectively. The reactive-transport model yielded k_{obs} values between 9.16 and 33.3 min^{-1}, which were 2 to 4 orders of magnitude higher than previously reported. PAC-Ti_4O_7 REM was tested with tap water spiked with 0.11 mg L^{-1} of nine different HAAs in a similar reduction experiment. The results indicated that all HAAs were reduced to <20 μg L^{-1}. Moreover, the total combined concentration of five regulated HAAs was lower than the regulatory limit (60 μg L^{-1}). Density functional theory simulations suggest that a direct electron transfer reaction was the probable rate-determining step for HAA reduction.

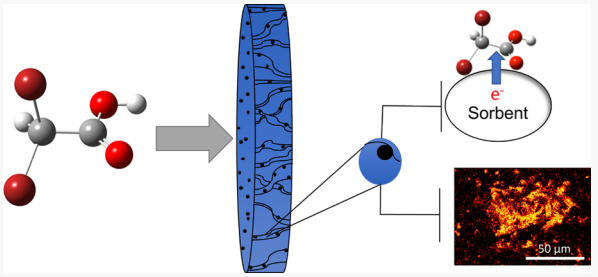

1. INTRODUCTION

Haloacetic acids (HAAs) are a group of water contaminants that are primarily produced during drinking water and wastewater chlorination. The suite of chemicals contains different halogen substituents (i.e., Cl, Br, and I). The toxicity of HAAs was investigated on male mice in previous studies, which suggested that dichloroacetic acid (DCAA) and trichloroacetic acid (TCAA) may be responsible for hepatic tumor formation in the liver.[1,2] Due to potential human health concerns, the U.S. Environmental Protection Agency (EPA) has regulated five HAAs (HAA_5), including monochloroacetic acid (MCAA), DCAA, TCAA, monobromoacetic acid (MBAA), and dibromoacetic acid (DBAA), with a combined concentration of <60 μg L^{-1} in drinking water.[3] The reaction between organic carbon in the water sources and chlorine-based water disinfectants is the most notable cause of HAA formation.[4] In addition, the presence of Br^- in water during chlorination can result in Br-containing HAA formation.[5] Several HAAs have also been detected in air,[6] swimming pool water,[7,8] rainwater,[9,10] and river water.[11]

Destructive methods for remediation of halogenated compounds have been found to be a reliable approach to decreasing their risks and thus have been investigated in numerous research studies.[12−15] Methods include but are not limited to sonoelectrochemical methods,[16] photocatalysis,[17,18] biodegradation,[19−21] and electrochemical oxidation and reduction with various electrodes and electrocatalysts (e.g., carbon material, Au, and Pd).[22−27] Application of these methods is limited by high capital and energy costs (photocatalysis and sonochemical methods), high capital costs (electrochemical methods), and special culture requirements for biodegradation methods (e.g., preparation of free cells, immobilization of specific bacteria, and protein purification).

Electrochemical methods have shown promising results to transform halogenated water contaminants to nontoxic compounds.[28,29] However, most previous studies utilize precious metals such as Pd (∼$1700 per ounce)[30] or expensive boron-doped diamond (BDD) electrodes (∼$7000 per m^2),[31] which poses a significant barrier to employ these methods broadly. By contrast, the application of Ti_4O_7, a conductive Magnéli phase of TiO_2, is inexpensive (e.g., ∼$0.36 per m^2 for laboratory-scale synthesis),[31] and it has shown exceptional performance as either an anode or cathode for the elimination of various groups of water contaminants.[32−36] However, a recent study showed that Ti_4O_7 electrodes do not have a significant adsorption capacity for polar water contaminants (e.g., *N*-nitrosodimethylamine (NDMA)), which can limit the removal efficiency when utilized in a single-pass operational mode.[32] Therefore, the addition of low-cost conductive carbon

Received: November 7, 2019
Revised: December 23, 2019
Accepted: December 26, 2019
Published: December 26, 2019

https://dx.doi.org/10.1021/acs.est.9b06744
Environ. Sci. Technol. 2020, 54, 1982−1991

adsorbents to Ti_4O_7 is expected to increase the dehalogenation performance.[37−39]

In this study, carbon-Ti_4O_7 composite reactive electrochemical membranes (REMs) were prepared from Ti_4O_7 powder and amended with either powder activated carbon (PAC) or multiwalled carbon nanotubes (MWCNTs) to increase the adsorption capacity of the REMs for HAAs. The prepared REMs were characterized for their physical properties and tested in a single-pass flow-through reactor to investigate the performance of the carbon-composite REMs for simultaneous adsorption and reduction of HAAs in synthetic and tap water solutions. A reactive transport model was used to interpret the experimental data, and density functional theory (DFT) simulations were used to investigate possible reaction mechanisms.

2. MATERIALS AND METHODS

2.1. Reagents. The mixture of nine HAAs (HAA_9) was obtained from Restek Corporation (Bellefonte, PA), which include bromochloroacetic acid (BCAA), bromodichloroacetic acid (BDCAA), chlorodibromoacetic acid (CDBAA), dibromoacetic acid (DBAA), dichloroacetic acid (DCAA), monobromoacetic acid (MBAA), monochloroacetic acid (MCAA), tribromoacetic acid (TBAA), and trichloroacetic acid (TCAA). All other reagents were obtained from Sigma-Aldrich (St. Louis, MO), Fisher Scientific (Pittsburgh, PA), and VWR International (Radnor, PA). All gases were of ultrahigh purity grade (UHP) and were obtained from Praxair (Danbury, CT). All solutions were prepared with deionized (DI) water, which was obtained from a Barnstead NANO pure water system (18.2 MΩ cm at 25 °C). All reagents were used as received without additional purification.

2.2. Fabrication of Ti_4O_7 Electrodes. The Ti_4O_7 REMs and carbon-Ti_4O_7 REMs were fabricated according to recently reported methods.[32] The carbon-Ti_4O_7 composites were fabricated with MWCNTs or PAC to increase their adsorption capacity for HAA_9. The three electrodes used in this study were labeled as follows: REM (100% Ti_4O_7), MWCNT-REM (90% Ti_4O_7/10% MWCNTs), and PAC-REM (90% Ti_4O_7/10% PAC). All electrodes were cylindrical in shape with a 1 cm^2 surface area, 2 mm thickness, and 30% porosity.

2.3. Physical Characterization. Cross-sectional scanning electron microscopy−energy dispersive X−ray spectroscopy (SEM-EDS; SEM: Hitachi S-3000N VPSEM, Schaumburg, IL; EDS: Oxford Inca EDS system with a light element Si(Li) X-ray detector, High Wycombe, U.K.) and cross-sectional Raman spectroscopy (alpha300 RA, WITec, Ulm, Germany) were performed to characterize the morphology and spatial elemental distribution of the carbonaceous materials in the REMs.

2.4. Analytical Methods. HAA_9 compounds (BCAA, BDCAA, CDBAA, DBAA, DCAA, MBAA, MCAA, TBAA, and TCAA) were analyzed following EPA method 552.3.[40] Briefly, 3 mL water samples were adjusted to a pH of <0.5 with sulfuric acid (18 M) and extracted with 3 mL of methyl *tert*-butyl ether (MTBE). 1,2,3-Trichloropropane was used as the internal standard. The extracted HAA_9 was converted to methyl esters by adding 2 mL of 10% sulfuric acid in methanol (18 M) and reacted at 50 °C for 2 h. An aliquot of 5 mL of a 150 g L^{-1} Na_2SO_4 solution was added to remove the acidic aqueous phase, and 0.75 mL of a saturated $NaHCO_3$ solution was used to neutralize the solution. The extracts were then analyzed by gas chromatography with an electron capture detector (GC-ECD), where an Rxi-5ms column (30 m × 0.25 mm, 0.25 μm; Restek Inc., Bellefonte, PA) was used with N_2 as the carrier gas. Instrumental method details are provided in the Supporting Information. Solid-phase extraction of HAA_9 from REM, MWCNT-REM, and PAC-REM was performed to complete the mass balance (see the Supporting Information). The concentration of Br^- and DBAA from batch reactors with an elevated initial concentration of 250 μM was analyzed by ion chromatography (IC) (Dionex, ICS-2100). For all liquid chromatographic methods, the analytical standards were prepared in the background electrolytes used in the experiments.

2.5. Adsorption Isotherm Analysis. The Ti_4O_7, PAC-Ti_4O_7, and MWCNT-Ti_4O_7 powders were tested in batch adsorption experiments (without applied potentials) to construct adsorption isotherms of HAAs. The solid-phase concentrations of HAAs were calculated using a mass balance approach by determining the change in aqueous concentration of HAAs after 24 h when the adsorption equilibrium was achieved. Kinetic adsorption tests were performed to verify that this time frame was sufficient (see Figure S1, Supporting Information).

2.6. REM Flow-Through and Batch Reactors. A flow-through reactor was used for conducting adsorption/electrochemical reduction experiments for DBAA and HAA_9, and a batch reactor was used to conduct experiments for calculation of the enthalpies of activation ($\Delta H^{\ddagger}$) for electrochemical reduction of DBAA. The flow-through reactor was operated in the up-flow direction in which the feed solution was pumped first through a 0.5 cm^2 REM disk cathode (working electrode) followed by a 0.33 cm^2 316 stainless-steel anode (counter electrode). A 1 mm Ag/AgCl reference electrode (LF-100, Warner Instruments, Hamden, CT) was placed ∼1 mm from the working electrode (Figure S2, Supporting Information). A digital gear pump (model no. 75211-70, Micropump, Vancouver, WA) and a Gamry potentiostat/galvanostat (Gamry Instruments, Warminster, PA) were used to perform the experiments. The solution resistance between the reference and working electrodes was measured, and all potentials were corrected and reported versus the standard hydrogen electrode (SHE). The permeate flux was held constant at 200 L m^{-2} h^{-1} (LMH), which provided a liquid residence time of ∼11 s in the REMs.

Adsorption and reduction experiments of DBAA alone and a mixture of HAA_9 compounds were carried out using all three REMs in the flow-through reactor. A feed solution of 1 mg L^{-1} DBAA was prepared in 10 mM KH_2PO_4/K_2HPO_4 (pH 7). Additional experiments were conducted with tap water spiked with the HAA_9 mixture (each compound at 0.11 mg L^{-1}), and the PAC-REM was used to evaluate its performance for the treatment of contaminated drinking water. For adsorption experiments, each REM was tested under open-circuit potential (OCP) conditions. After obtaining the HAA breakthrough curves and achieving saturation of the sorbents, cathodic potentials between −1.1 and −1.5 V/SHE were applied, and permeate concentrations were analyzed over time. The reduction experiments were carried out for 45 h. All experiments were conducted in duplicate and at room temperature (∼22 °C). Error bars in all figures and errors reported in the text represent 95% confidence intervals of mean values.

The batch reactor was a divided-cell, jacketed, glass reactor (Figure S3, Supporting Information). A Nafion A115

https://dx.doi.org/10.1021/acs.est.9b06744
Environ. Sci. Technol. 2020, 54, 1982−1991

membrane (Ion Power, Inc., New Castle, DE) was used as a separator of anode and cathode chambers. The REM was placed in a custom-made rotating disk electrode (RDE) holder and rotated at 5000 rotations per minute (RPM). The Ag/AgCl reference electrode was placed ~2 mm from the working electrode, and a Pt wire (Alfa Aesar, Tewksbury, MA) was used as a counter electrode and placed in the anode chamber. A recirculating water bath (NESLAB RTE 7, Thermo Fisher Scientific, Grand Island, NY) was used to control temperatures at 15, 20, 25, and 30 °C. Three sets of experiments at cathodic potentials of −1.1, −1.5, and −1.8 V/SHE were carried out at each temperature to calculate the experimental $\Delta H^{\ddagger}$ values according to the Arrhenius equation.

2.7. Transport Simulations. Mathematical reactive transport simulations were used to estimate DBAA adsorption and reaction in the REM system, according to eq 1.

$$R\frac{\partial \overline{C}}{\partial T} = \frac{1}{Pe}\frac{\partial^2 \overline{C}}{\partial \overline{X}^2} - \frac{\partial \overline{C}}{\partial \overline{X}} - \overline{k}\overline{C} \tag{1}$$

The parameter R is known as the retardation factor and is given by eq 2.

$$R = 1 + \frac{\rho_b}{\theta}(nK_F C^{(n-1)}) \tag{2}$$

In these equations, $\overline{C}$ $\left(\overline{C} = \frac{C}{C^0}\right)$, T $\left(T = \frac{tu}{L}\right)$, $\overline{X}$ $\left(\overline{X} = \frac{x}{L}\right)$, $\overline{k}$ $\left(\overline{k} = \frac{k_{obs}L}{u}\right)$ are the dimensionless concentration, time, length, and kinetic rate constant, respectively; Pe $\left(Pe = \frac{uL}{D_a}\right)$ is the Peclet number; L is the REM thickness ($L = 2.0 \times 10^{-3}$ m); C_0 is the feed concentration; C and q are the concentrations in the aqueous and solid phases, respectively; u is the pore velocity of the fluid ($u = 1.85 \times 10^{-4}$ m s^{-1}); D_a is the axial dispersion coefficient; ρ_b is the bulk density of the available adsorbent phase; θ is the REM porosity ($\theta = 0.3$); k_{obs} is the observed pseudo-first-order reaction rate constant; x is the depth into the REM; t is the time; K_F is the Freundlich adsorption constant; and n is the exponent of nonlinearity. Equation 1 was solved using the pdep solver in MATLAB (R2016b) with the following initial and boundary conditions:

$$\overline{C}(T = 0) = 0 \quad 0 < \overline{X} < 1 \quad \text{(adsorption experiments)} \tag{3a}$$

$$\overline{C}(T = 0) = 0 \quad 0 < \overline{X} < 1 \quad \text{(reduction experiments)} \tag{3b}$$

$$\overline{C}(\overline{X} = 1) = C_0 \quad T \geq 0 \tag{4}$$

$$\frac{\partial \overline{C}(\overline{X} = 1)}{\partial \overline{X}} = 0 \quad T \geq 0 \tag{5}$$

More details regarding the mathematical model derivation are provided in the Supporting Information.

2.8. Quantum Mechanical Simulations. Density functional theory (DFT) calculations utilized the Gaussian 16 software.[41] Unrestricted spin, all-electron calculations were performed using the 6-311G++(d) basis set for frequency, geometry optimization, and energy calculations. The M06-2X hybrid meta exchange-correlation functional was used for all calculations.[42] Implicit water solvation was simulated using the SMD model.[43] Explicit water molecules were not incorporated into simulations as initial calculations indicated that hydrogen bonding was unimportant for the molecules investigated.

The E^0 values for a given direct electron transfer reaction were calculated by the following equation

$$E^0 = -\frac{\Delta_r G^0}{nF} - E^0_{abs}(\text{SHE}) \tag{6}$$

where $\Delta_r G^0$ is the Gibbs free energy for the reduction reaction, F is the Faraday constant, n is the number of electrons transferred, and E^0_{abs}(SHE) is a reference value for the absolute standard reduction potential of the SHE (4.28 eV).[44,45] Calculation results found that $\Delta H^0 \approx E^0$ (i.e., within ±|0.12| V difference) due to small entropic contributions to the Gibbs reaction energy. Therefore, potential-dependent $\Delta H^{\ddagger}$ values for direct electron transfer reduction reactions were determined using a Marcus-type relationship, as follows[46]

$$\Delta H^{\ddagger} = \frac{\lambda_H}{4}\left[1 + \frac{96.5(E - E^0)}{\lambda}\right]^2 \tag{7}$$

where E is the applied electrode potential, and λ_H is the enthalpic contribution to the total reorganization energy of the reduction reaction. The ratios of the reorganization energies for the forward and reverse reactions ($\Lambda = \lambda_{H,f}/\lambda_{H,r}$) were calculated to check the validity of using Marcus theory, where Λ should be ~1.0.

2.9. Energy Calculations. The electrical energy per order (E_{EO}) (kWh m^{-3}) was calculated using the following equation

$$E_{EO} = 10^{-3} \times \frac{V_{cell} I}{Q \log\left[\frac{C_f}{C_p}\right]} \tag{8}$$

where C_f is the compound feed concentration, C_p is the compound permeate concentration, V_{cell} is the cell potential (V), I is the current (A), and Q is the volumetric permeate flow rate (m^3 h^{-1}). The electrical energy consumption per gram of compound degraded (EC) (kWh g^{-1}) was calculated using eq 9.

$$\text{EC} = \frac{V_{cell} I}{Q(C_f - C_p)} \tag{9}$$

In eq 9, concentrations are in mg L^{-1}.

The required energy for pumping the feed through the membrane (E_Q, kWh m^{-3}) was calculated by eq 10

$$E_Q = (3.6 \times 10^{-6})\frac{\rho g \Delta P}{\eta} \tag{10}$$

where ρ is the water density, g is the gravitational constant, ΔP is the transmembrane pressure, η is the pump efficiency (assumed 0.7), and 3.6×10^{-6} is the conversion factor from joules to kWh.

3. RESULTS AND DISCUSSION

3.1. Physical Characterization. The physical properties of the three REMs were characterized in a previous study.[32] Results indicated that the REMs contained high-purity Ti_4O_7, and Raman spectroscopy analysis indicated that the carbonaceous content was not sufficiently altered during the synthesis process.[32] The average DI water permeabilities were 806 ± 14 LMH bar^{-1} for REM, 589 ± 16 LMH bar^{-1} for PAC-REM, and 290 ± 13 LMH bar^{-1} for MWCNT-REM.[32] Conductivity measurements were 935 ± 14 S m^{-1} for REM, 1832 ± 19 S m^{-1} for PAC-REM, and 2991 ± 37 S m^{-1} for MWCNT-

https://dx.doi.org/10.1021/acs.est.9b06744
Environ. Sci. Technol. 2020, 54, 1982−1991

REM.[32] The effective average pore sizes for REM, PAC-REM, and MWCNT-REM were 0.35 ± 0.05, 0.30 ± 0.04, and 0.20 ± 0.04 μm, respectively.[32]

Cross-sectional analysis of the REMs using SEM-EDS was performed to characterize the structural morphology and elemental composition as a function of depth into the REMs. To conduct this analysis, vertical cross sections of each REM were prepared, and three positions were defined and analyzed: 0 mm from the surface (top), 1 mm from the surface (middle), and 2 mm from the surface (bottom). The SEM images for the REMs showed the typical porous structure observed in prior studies (Figure 1 and Figure S4).[34] SEM-EDS analyses showed

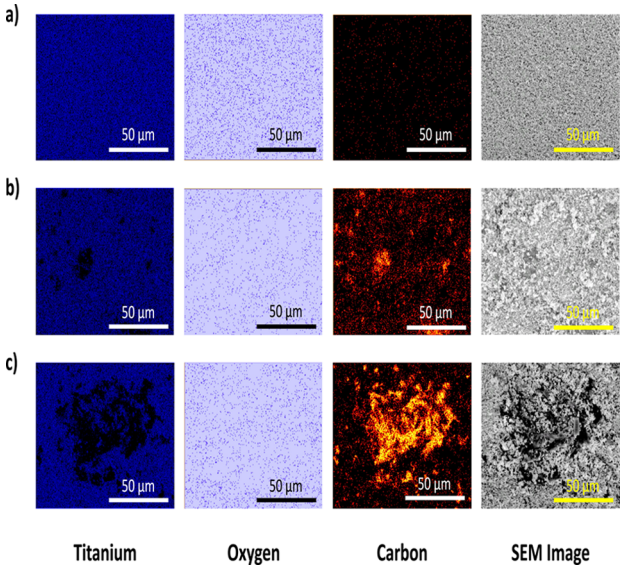

Figure 1. Cross-sectional scanning electron microscopy−energy dispersive X-ray spectroscopy (SEM-EDS) of (a) REM, (b) MWCNT-REM, and (c) PAC-REM. Elemental mapping attributed to each scanned region was obtained for titanium, oxygen, and carbon. Scale bars are the same for all panels. See the Supporting Information for the other regions on the top and bottom of the REMs and the distribution graphs for each element.

that the distribution of the carbon was present throughout the Ti_4O_7 matrix, with some carbon segregation detected for both MWCNT-REM and PAC-REM. Figure 1 shows the SEM-EDS data from the middle of the REMs, and other data are provided in Figures S4 and S5 (Supporting Information). Images from the three locations showed similar results, indicating that fairly uniform distribution of carbon throughout the REM samples was achieved. Trace levels of well-dispersed carbon were detected in the Ti_4O_7 REM, which was attributed to carbon contamination from the environment. The EDS analysis of the PAC-REM detected other trace elements (i.e. Mg, Si, and K), which was attributed to constituents present in the PAC powder as they were not seen in other REM samples. See Figures S4−S8 (Supporting Information) for details of spectra and images for all regions of the samples.

Raman spectroscopy was also used to spatially characterize the carbonaceous materials in the PAC-REM and MWCNT-REM. Cross-sectional Raman analysis was performed on five different spots (i.e., 0, 0.5, 1.0, 1.5, and 2.0 mm) from top to bottom of the REMs (Figure 2). For the REM sample, neither D nor G peaks related to carbon compounds were observed, as expected. Characteristic D and G peaks were observed at

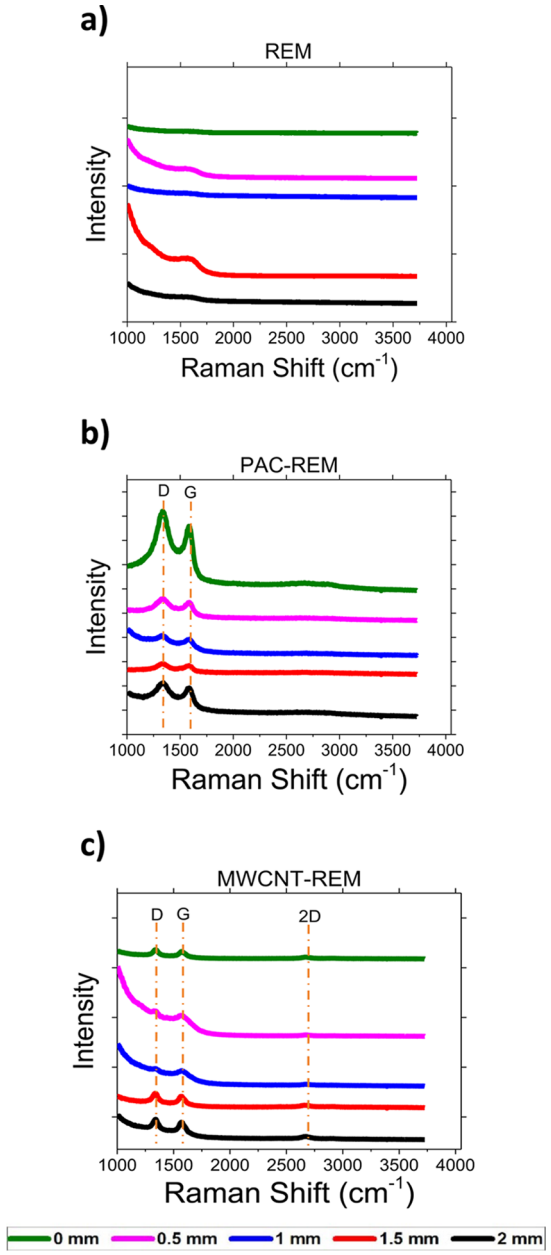

Figure 2. Cross-sectional Raman spectroscopy from top to bottom for (a) REM, (b) PAC-REM, and (c) MWCNT-REM. Both D and G peaks were observed for PAC in the standard region. For MWCNTs, a 2D peak was also observed. Each type of REM was analyzed by five spots from top to bottom.

Raman shift values of 1324−1341 and 1581−1589 cm^{-1} for PAC-REM and 1324−1341 and 1565−1573 cm^{-1} for MWCNT-REM, respectively. The characteristic 2D peak related to MWCNTs was observed at 2659−2673 cm^{-1} at different sample locations. The D/G intensity ratios were 1.11, 1.05, 1.04, 1.02, and 1.06 for PAC-REM from top to bottom and were 1.05, 1.1, 1.05, 1.08, and 1.07 for MWCNT-REM from top to bottom. The peak intensities varied between sampling points and was attributed to the non-uniform C distribution and the laser sampling size of 720 nm. Results showed the presence of the carbonaceous materials in the composites without substantial alteration either on the surface or in the bulk due to the synthesis methods and are in agreement with past works.[32,34,36]

https://dx.doi.org/10.1021/acs.est.9b06744
Environ. Sci. Technol. 2020, 54, 1982−1991

3.2. Adsorption Isotherms. The adsorption isotherms of HAA_6 are shown in Figure S9 (Supporting Information) for REM, PAC-REM, and MWCNT-REM. Three of the HAA_9 compounds were not stable, and some degradation occurred. Approximately 39, 6.4, and 1.3% of TBAA, CDBAA, and BDCAA disappeared during the experimental time frame of 24 h, respectively. By contrast, appreciable loss was not observed for the other HAAs (HAA_6: MCAA, DCAA, TCAA, MBAA, DBAA, and BCAA) in 24 h, which is consistent with a previous study.[39] As such, the present study proceeded with HAA_6, all of which exhibited nonlinear sorption behavior and fit the Freundlich model (eq 11)

$$q = K_F C_e^n \tag{11}$$

where q (mg g^{-1}) and C_e (mg L^{-1}) are the adsorbed and aqueous concentrations of HAA_6 at equilibrium, respectively. Results from the isotherm fitting are summarized in Figure S9 and Table S1 (Supporting Information). In general, as the number of halogen substituents (−Cl or −Br) increased, K_F values increased (MCAA < DCAA < TCAA), while n values decreased (MCAA > DCAA > TCAA). The decrease in n values suggests that the interaction between HAA_6 and carbonaceous materials becomes stronger as the number of halogen atoms increases, possibly resulting in the higher adsorption capacity. Similar trends were observed for HAA_6 on granular activated carbon (GAC) in a previous study.[47] In all cases, the n values were less than 1.0, indicating that the adsorption process was a physical process.[48] Furthermore, n < 1 was attributed to a decrease in bonding energies between adsorbent and adsorbate phases as a result of multilayer adsorption and heterogeneous adsorption sites.[49] The HAA_6 exhibited higher adsorption capacities toward MWCNT-REM followed by PAC-REM and REM. We postulate that the larger surface area of MWCNTs and PAC with respect to REM contributed to their enhanced adsorption capacities.

3.3. Flow-Through Adsorption Experiments. DBAA was selected as a stable model compound to carry out adsorption and electrochemical reduction experiments and evaluate the carbon-Ti_4O_7 composite REMs, as control experiments indicated that it was a stable compound for reduction in the presence of unpolarized PAC and MWCNT powders for 24 h in batch mode (see Figure S10, Supporting Information). To acquire DBAA breakthrough curves, 1 mg L^{-1} solution of DBAA in 10 mM KH_2PO_4/K_2HPO_4 (pH 7) was prepared and tested with the three REMs under OCP conditions. The results indicated that the required bed volumes to reach 50% of the feed concentration were 703, 1900, and 6006 for REM, PAC-REM, and MWCNT-REM, respectively, indicating that the adsorption capacity of DBAA increased by 2.7-fold on PAC-REM and increased by 8.5-fold on MWCNT-REM relative to the REM (Figure 3). It should be noted that early breakthrough of DBAA was observed in the low bed volume data presented in Figure 3 with normalized concentrations of ∼0.1. These aqueous concentrations were attributed to short-circuiting of the liquid flow around the sealing gaskets of the REMs.

Average results from duplicate experiments and transport model fits (eq 1) are included in Figure 3a,c. Model simulations utilized Pe = 10, which was determined by conservative tracer data obtained with a 1 mM $NaClO_4$ solution (see Figure S11, Supporting Information). The transport model was fit to the adsorption data by using the values obtained from the batch isotherm parameters (i.e., K_F and n), setting $\bar{k} = 0$, and fitting a value for ρ_b. For the case of the REM, DBAA batch adsorption experiments did not yield reliable isotherm data due to negligible adsorption. Therefore, an average value of R = 9.1 was fit to the data (Figure 3a). Fitting the transport model to the experimental data yielded values of ρ_b = 138 g L^{-1} (∼46% of total C added) for MWCNT-REM (Figure 3b) and ρ_b = 31.4 g L^{-1} (∼10% of total C added) for PAC-REM (Figure 3c). These results indicated that the MWCNTs were more available for adsorption reactions than the PAC within the Ti_4O_7 matrix, which is similar to findings in our previous study.[32]

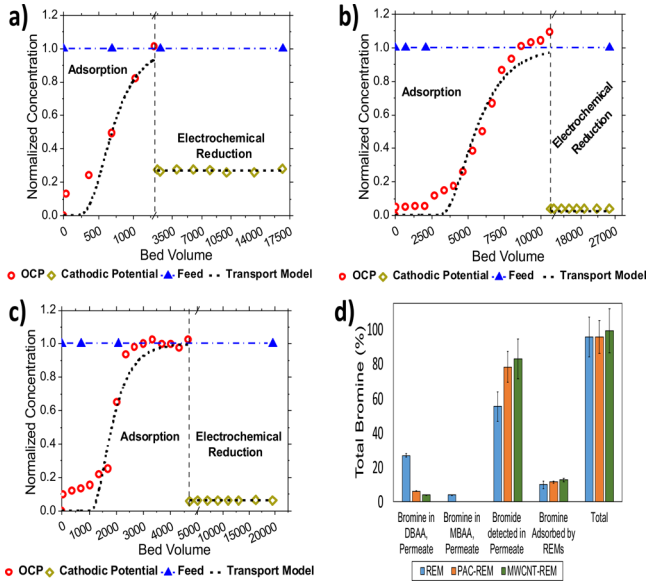

Figure 3. Adsorption and electrochemical reduction results of 1 mg L^{-1} DBAA in 10 mM KH_2PO_4/K_2HPO_4 for (a) REM, (b) MWCNT-REM, and (c) PAC-REM at cathodic polarization of −1.5 V/SHE. Each graph represents an average value of duplicate experiments. (d) Total bromine analysis for permeate samples after reduction experiments using all types of REMs.

3.4. Electrochemical Dehalogenation of HAAs. Dehalogenation of HAAs with the carbon REMs was used under cathodic polarizations instead of anodic polarization because a past work indicated that the carbonaceous material in the REM was not stable during anodic polarization.[32] Flow-through experiments were first conducted with 1 mg L^{-1} DBAA in 10 mM KH_2PO_4/K_2HPO_4 at a potential of −1.1 V/SHE with PAC-REM, and negligible removal was observed (see Figure S12, Supporting Information). Therefore, the potential was increased to −1.5 V/SHE with J = 200 LMH, and ∼94% removal of DBAA was achieved. Figure 3 shows the average concentration profiles from duplicate experiments for the reduction of 1 mg L^{-1} DBAA on the three REMs. The results from duplicate experiments showed steady-state removal values of 70.7 ± 0.1% and 75.3 ± 0.5% for REM, 92.2 ± 0.2% and 95.8 ± 0.01% for PAC-REM, and 94.7 ± 0.01% and 97.8 ± 0.01% for MWCNT-REM. Average values of these duplicate experiments are shown in Figure 3. The steady-state permeate concentrations observed with the application of cathodic potentials indicated that adsorption site saturation was not occuring and the treatment strategy could operate as a continuous process without the need for offline adsorbent regeneration. Results also indicated that the DBAA concentrations in the permeate after reduction were 268 ± 7.8 μg L^{-1} for REM, 59 ± 1.3 μg L^{-1} for PAC-REM, and 37.5 ± 0.1 μg

https://dx.doi.org/10.1021/acs.est.9b06744
Environ. Sci. Technol. 2020, 54, 1982−1991

L^{-1} for MWCNT-REM. The permeate concentrations for the PAC-REM and MWCNT-REM were lower than the EPA regulation (60 μg L^{-1}) for HAA_5 (MCAA, DCAA, TCAA, MBAA, and DBAA) in drinking water.[3]

Fitting of the transport model to the reduction data utilized the previously determined parameters to fully describe R and varied $\overline{k}$ $\left(\overline{k} = \frac{k_{obs}L}{u}\right)$. Values of $\overline{k}$ = 1.65 (k_{obs} = 9.16 min^{-1}) for REM (Figure 3a), $\overline{k}$ = 6.0 (k_{obs} = 33.3 min^{-1}) for MWCNT-REM (Figure 3b), and $\overline{k}$ = 3.3 (k_{obs} = 18.3 min^{-1}) for PAC-REM (Figure 3c) were obtained. By comparison, k_{obs} for DBAA reduction using elemental iron (Fe^0) was reported as 0.014 min^{-1}.[50] Recent works have reported k_{obs} values between 0.03 and 0.58 min^{-1} for TCAA electrochemical reduction in batch mode,[25,26,51−53] which are approximately 57 to 1110 times lower than our results with the MWCNT-REM. The very high rate constants observed in our study were attributed to the high surface area and efficient mass transport of the flow-through reactor. The increase in the rate constants by a factor of 3.6 for MWCNT-REM and 2.0 for PAC-REM relative to the REM was attributed to the increased adorption capacity due to carbon addition.

Figure 3d shows the total bromine mass balance of the DBAA dehalogenation experiments for the three REMs. The results showed Br^- release and trace MBAA formation during DBAA reduction on the REM. The further oxidation of Br^- was not observed on the anode. Most likely due to the short hydraulic residence time on the low-surface area (0.33 cm^2) planar electrode. MBAA formation was not seen in the reduction experiments with PAC-REM and MWCNT-REM. Solid-phase extraction to detect adsorbed DBAA and other Br-containing compounds was performed on the REMs after the experiments to complete the bromine mass balance. Unidentified Br-containing compounds adsorbed on the REMs were oxidized to BrO_3^- and are reported in Figure 3d as "Bromine Adsorbed by REMs". Results indicated that only small amounts of DBAA were extracted back from the PAC-REM (0.6 μg) and MWCNT-REM (0.3 μg). Most of the adsorbed Br was from other unindentified compounds (99.5−99.7%), see Table S2. The total Br mass balance, calculated as the ratio of bromine concentrations in DBAA and its transformation products over the intitial DBAA ((2 × [DBAA] + [MBAA] + [Br^-] + [Br Adsorbed])/(2 × $[DBAA]_0$) × 100), was 95.5 ± 11.6% for REM, 95.3 ± 9.7% for PAC-REM, and 98.9 ± 12.5% for MWCNT-REM. The lack of significant HAA reduction products in the permeate, low concentration of adsorbed DBAA (0.03−0.05% of total feed mass), low concentration of other Br-containing products (10−12% of total feed mass), and the near 100% mass balances indicated the effectiveness of the REMs for DBAA reduction.

To test the carbon-Ti_4O_7 REMs with a realistic drinking water treatment scenario, a solution of 0.11 mg L^{-1} of each HAA_9 was added to tap water (ionic strength, 2 mM; see Table S3, Supporting Information, for tap water composition) without the addition of a background electrolyte. This solution was tested at −1.5 V/SHE cathodic polarization and 200 LMH flow rate with the PAC-REM in flow-through mode. The PAC-REM was selected over the MWCNT-REM due to the low cost of PAC and concerns over the potential release of MWCNTs to drinking water.[54−57] The tap water spiked with HAA_9 solution was fed to the PAC-REM for 50 h, and concentration analysis was performed on permeate samples. Results showed that the HAA concentrations decreased from 111 to <20 μg L^{-1} for all of the HAA_9 compounds over the duration of the 2 day experiments. The lowest concentration was for TCAA with a concentration of 6.0 ± 0.5 μg L^{-1}, and the highest one was TBAA with a concentration of 16 ± 0.1 μg L^{-1}. Figure 4 shows the reduction results for the HAA_9-spiked

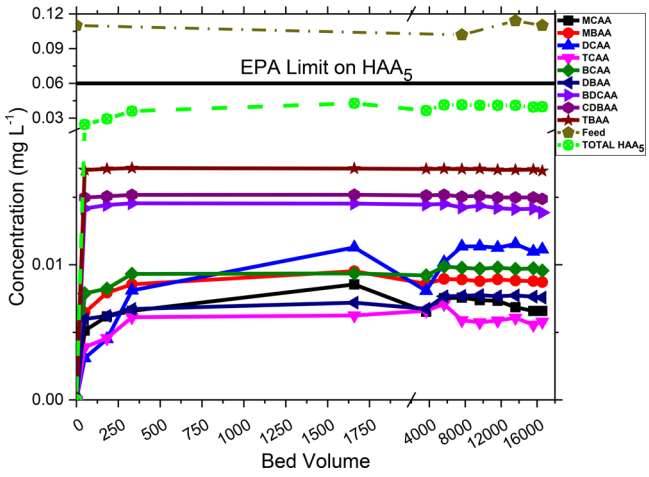

Figure 4. Electrochemical reduction results for a mixture of HAA_9 at a concentration of 0.11 mg L^{-1} each in tap water (ionic strength, 2 mM) for PAC-REM at a cathodic potential of −1.5 V/SHE.

tap water experiment. A control experiment was conducted without an applied potential and showed that near complete breakthrough of all HAA_9 compounds (Figure S13, Supporting Information), indicating that nonelectrochemical reactions (e.g., hydrolysis) were not a significant removal pathway under these short hydraulic residence times (~11 s). The combined concentration of HAA_5 (MCAA, DCAA, TCAA, MBAA, and DBAA) was 37.9 ± 3.5 μg L^{-1}, which was lower than the EPA maximum contaminant level of 60 μg L^{-1} for HAA_5,[3] with a hydraulic residence time of only 11 s. By contrast, a recent study of electrochemical reduction of HAA_5 from an initial concentration of 120 to <60 μg L^{-1} required approximately a 15 min hydraulic residence time.[26]

The reduction results of either DBAA or mixture of HAA_9 showed significant removal from water using the carbon-Ti_4O_7 REMs. The carbon-Ti_4O_7 composites were able to increase the removal of HAAs from 73.0 ± 0.65% on REM to 94.0 ± 0.13% on PAC-REM and 96.2 ± 0.05% on MWCNT-REM. Both composite REMs were able to decrease the HAA concentrations to <60 μg L^{-1} and showed that they could effectively reduce HAAs from water.

3.5. Reaction Mechanism. Studies have investigated the primary mechanisms for electrochemical HAA reduction by utilizing experimental techniques, and it is generally thought that HAA reduction occurs through either direct electron transfer or atomic hydrogen reduction.[26,51] The hydrogen reduction mechanism is thought to be dominant when a hydrogenation catalyst (e.g., Pd and Ni) is a component of the cathode material, and direct electron transfer is dominant for nonprecious metal cathodes.[26] Therefore, simulations were conducted to determine the E^0 and the potential-dependent $\Delta H^{\ddagger}$ values for the direct electron reduction reactions of all HAA_9 compounds studied in this work, according to eqs 6 and 7, respectively. The general concerted reduction reaction is shown below

$$R - X + e^- \rightarrow R + X^- \quad (12)$$

https://dx.doi.org/10.1021/acs.est.9b06744
Environ. Sci. Technol. 2020, 54, 1982−1991

where X is a halide atom. The E^0, ΔH^0, λ_H, and Λ values are listed in Table 1. Marcus theory assumes similar potential energy surfaces for the reactant and product, which requires $\Lambda \approx 1.0$. These conditions were approximately met for these simulations, with Λ values ranging from 1.09 to 1.39 for the HAA_9 (Table 1). In general, the E^0 values were the most negative for the monohalogenated compounds and the least negative for the trihalogenated compounds. These results were attributed to the electron-withdrawing capacity of the halogens, where multiple halogens increased the partial positive charge on the carbon atoms and thereby allowed the electron transfer reaction to occur at lower cathodic potentials. Brominated and chlorinated HAAs with the same number of halogen atoms had very similar E^0 values to each other but more significant differences in their λ_H values (Table 1), where the combination of these two parameters ultimately determines the potential dependent $\Delta H^{\ddagger}$ and free energy of activation ($\Delta G^{\ddagger}$) values.

Table 1. Results from DFT Simulations[a]

Compound	E^0 (V/SHE)	ΔH (V/SHE)	λ_H (kJ mol^{-1})	Λ
MBAA	−1.04	−1.12	237	1.09
DBAA	−0.68	−0.80	219	1.28
TBAA	−0.37	−0.49	207	1.33
MCAA	−0.97	−1.06	300	1.28
DCAA	−0.64	−0.73	259	1.39
TCAA	−0.29	−0.40	227	1.13
BCAA	−0.66	−0.77	267	1.16
DBCAA	−0.34	−0.43	−234	1.13
DCBAA	−0.32	−0.45	203	1.28

[a]MBAA, monobromoacetic acid; DBAA, dibromoacetic acid; TBAA, tribromoacetic acid; MCAA, monochloroacetic acid; DCAA, dichloroacetic acid; TCAA, trichloroacetic acid; BCAA, bromochloroacetic acid; DBCAA, dibromochloroacetic acid; DCBAA, dichlorobromoacetic acid.

The potential-dependent $\Delta H^{\ddagger}$ and $\Delta G^{\ddagger}$ profiles are shown in Figure 5 for HAA_9. It should be noted that the $\Delta H^{\ddagger}$ and $\Delta G^{\ddagger}$ profiles for a given compound are very similar, thereby justifying the use of a Marcus-type relationship for $\Delta H^{\ddagger}$ calculations (eq 7). The $\Delta H^{\ddagger}$ and $\Delta G^{\ddagger}$ values were higher for the chlorine-substituted HAAs relative to the bromine-substituted HAAs with the same number of halogen atoms, which is consistent with past research.[58] This result is due to the higher reorganization energy for chlorine-containing compounds relative to bromine-containing compounds (Table 1). To provide supporting evidence for the direct electron transfer mechanism, experimental $\Delta H^{\ddagger}$ values were calculated using the Arrhenius equation (see Figures S14−S16, Supporting Information), and the data are included on Figure 5b. The general agreement between experimental and

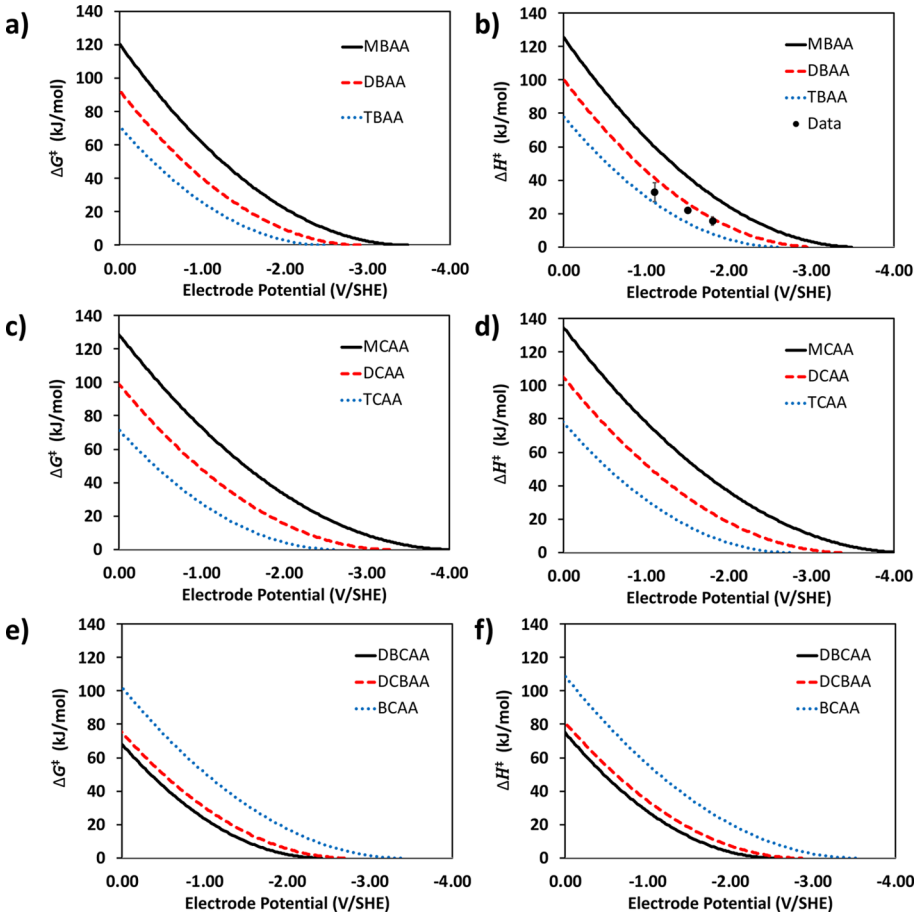

Figure 5. Results for DFT-calculated $\Delta G^{\ddagger}$ (a, c, e) and $\Delta H^{\ddagger}$ (b, d, f) values as a function of electrode potential. Panel (b) includes data points for experimental enthalpy $\Delta H^{\ddagger}$ measurements. MBAA, monobromoacetic acid; DBAA, dibromoacetic acid; TBAA, tribromoacetic acid; MCAA, monochloroacetic acid; DCAA, dichloroacetic acid; TCAA, trichloroacetic acid; BCAA, bromochloroacetic acid; DBCAA, dibromochloroacetic acid; DCBAA, dichlorobromoacetic acid.

https://dx.doi.org/10.1021/acs.est.9b06744
Environ. Sci. Technol. 2020, 54, 1982−1991

theoretical $\Delta H^{\ddagger}$ values suggests that direct electron transfer was the likely rate-determining mechanism responsible for DBAA reduction, and these results should be analogous for other HAAs.

3.6. Technical and Environmental Significance. The analysis related to reduction of either DBAA or HAA_9 showed significant removal of these compounds by using carbon-Ti_4O_7 cathodes. Similar to a previous work for NDMA,[32] increasing adsorption in the composites due to existence of the carbonaceous materials had a significant effect on the removal performance of the REMs. Previous studies on electrochemical reduction of the HAAs were carried out by using costly catalysts (e.g., Pd and Au) and high-conductivity electrolytes (e.g., 0.1−0.5 M)[22,23] or employing common metallic catalysts (e.g., Co and Fe) in an acidic environment (pH 5.6)[27] to increase the kinetics of HAA removal. Most of the previous studies focused on one or a selected group of HAAs (mostly chloroacetic acids)[24,26] and did not consider the other HAAs. By contrast, our work provides a feasible remediation method for a range of HAAs with low-cost materials in low-conductivity, neutral pH solutions.

The energy usage for reducing DBAA in duplicate experiments was calculated as E_{EO} = 0.33 ± 0.05 kWh m^{-3} (EC = 0.37 kWh g^{-1}) and E_{EO} = 0.27 ± 0.04 kWh m^{-3} (EC = 0.30 kWh g^{-1}) for REM, E_{EO} = 0.19 ± 0.06 kWh m^{-3} (EC = 0.21 kWh g^{-1}) and E_{EO} = 0.33 ± 0.1 kWh m^{-3} (EC = 0.37 kWh g^{-1}) for PAC-REM, and E_{EO} = 0.30 ± 0.06 kWh m^{-3} (EC = 0.33 kWh g^{-1}) and E_{EO} = 0.22 ± 0.02 kWh m^{-3} (EC = 0.24 kWh g^{-1}) for MWCNT-REM. The energy usage for the tap water-spiked HAA_9 was calculated between E_{EO} = 0.10 and 0.14 kWh m^{-3} (EC = 0.11 to 0.16 kWh g^{-1}) (i.e., E_{EO} = 0.10 ± 0.07 kWh m^{-3} for MCAA, 0.11 ± 0.07 kWh m^{-3} for MBAA, 0.12 ± 0.07 kWh m^{-3} for DCAA, 0.10 ± 0.06 kWh m^{-3} for TCAA, 0.11 ± 0.06 kWh m^{-3} for BCAA, 0.10 ± 0.06 kWh m^{-3} for DBAA, 0.13 ± 0.08 kWh m^{-3} for BDCAA, 0.13 ± 0.08 kWh m^{-3} for CBDAA, and 0.14 ± 0.08 kWh m^{-3} for TBAA). Previous studies on electrochemical reduction of HAAs reported EC = 0.6 kWh g^{-1} for dechlorination of TCAA at a cathodic potential of −1.16 V/SHE on a Pd/graphene cathode.[25] Another study on a graphene-Cu cathode reported EC values as low as 0.067 kWh g^{-1} (E_{EO} = 0.15 kWh m^{-3}).[26] The required energy for pumping was calculated using eq 10, and E_Q = 0.01 kWh m^{-3} was obtained for the experimental conditions (i.e., J = 200 LMH, ΔP = 2.33 m of head), indicating that it was negligible in the overall energy consumption. Comparing electrochemical reduction to treat HAAs with other methods such as sonoelectrochemical treatment shows a significant higher energy requirement. Removing TCAA from water by the sonoelectrochemical method required energy usage between 600 and 810 kWh m^{-3} (~7000 times higher than the carbon-composite REMs).[16] Considering all of these results, it is apparent that elecrochemical reduction of HAAs on carbon-Ti_4O_7 REMs is an effecient and cost-effective treatment strategy. However, more work is needed to assess the long-term performance of the technologies in diverse water sources.

■ ASSOCIATED CONTENT

Supporting Information

The Supporting Information is available free of charge at https://pubs.acs.org/doi/10.1021/acs.est.9b06744.

Analytical methods, flow-through reactor schematic, transport model, details of SEM-EDS spectra and images for all types of REMs, adsorption isotherms results for HAA_6 (MCAA, DCAA, TCAA, MBAA, DBAA, and BCAA), ClO_4^- breakthrough curves for all types of REMs, supplementary DBAA electrochemical reduction flow-through experiments, DBAA extraction efficiencies for PAC and MWCNT powder, extraction of adsorbed species from REMs, tap water composition, and DBAA activation energy determination (PDF)

■ AUTHOR INFORMATION

Corresponding Author

Brian P. Chaplin − *University of Illinois at Chicago, Chicago, Illinois;* orcid.org/0000-0003-1668-5414; Phone: +13129960288; Email: chaplin@uic.edu

Other Authors

Soroush Almassi − *University of Illinois at Chicago, Chicago, Illinois*

Pamela Rose V. Samonte − *Villanova University, Villanova, Pennsylvania*

Zhao Li − *Villanova University, Villanova, Pennsylvania*

Wenqing Xu − *Villanova University, Villanova, Pennsylvania;* orcid.org/0000-0002-9838-8220

Complete contact information is available at: https://pubs.acs.org/10.1021/acs.est.9b06744

Notes

The authors declare no competing financial interest.

■ ACKNOWLEDGMENTS

Funding for this work was provided by the U.S. EPA National Center for Innovation in Small Drinking Water Systems under EPA agreement number RD 83560201-0 to W.X. and B.P.C., a National Science Foundation CAREER award to B.P.C. (CBET-1453081), and a National Science Foundation CAREER award to W.X. (CBET-1752220). The authors also acknowledge Dr. Vikas Berry and his research group for performing cross-sectional Raman analysis.

■ REFERENCES

(1) Herren-Freund, S. L.; Pereira, M. A.; Khoury, M. D.; Olson, G. The Carcinogenicity of Trichloroethylene and Its Metabolites, Trichloroacetic Acid and Dichloroacetic Acid, in Mouse Liver. *Toxicol. Appl. Pharmacol.* **1987**, *90*, 183−189.

(2) Bull, R. J.; Sanchez, I. M.; Nelson, M. A.; Larson, J. L.; Lansing, A. J. Liver Tumor Induction in B6C3F1 Mice by Dichloroacetate and Trichloroacetate. *Toxicology* **1990**, *63*, 341−359.

(3) United States Environmental Protection Agency. *Public Notification - Total Trihalomethanes (TTHM) and Haloacetic Acids (HAA5) MCL Template*; https://www.epa.gov/region8-waterops/public-notification-total-trihalomethanes-tthm-and-haloacetic-acids-haa5-mcl.

(4) Liang, L.; Singer, P. C. Factors Influencing the Formation and Relative Distribution of Haloacetic Acids and Trihalomethanes in Drinking Water. *Environ. Sci. Technol.* **2003**, *37*, 2920−2928.

(5) Heller-Grossman, L.; Manka, J.; Limoni-Relis, B.; Rebhun, M. Formation and Distribution of Haloacetic Acids, THM and TOX in Chlorination of Bromide-Rich Lake Water. *Water Res.* **1993**, *27*, 1323−1331.

(6) Frank, H.; Scholl, H.; Renschen, D.; Rether, B.; Laouedj, A.; Norokorpi, Y. Haloacetic Acids, Phytotoxic Secondary Air Pollutants. *Environ. Sci. Pollut. Res.* **1994**, *1*, 4−14.
(7) Righi, E.; Fantuzzi, G.; Predieri, G.; Aggazzotti, G. Bromate, Chlorite, Chlorate, Haloacetic Acids, and Trihalomethanes Occurrence in Indoor Swimming Pool Waters in Italy. *Microchem. J.* **2014**, *113*, 23−29.
(8) Cardador, M. J.; Gallego, M. Haloacetic Acids in Swimming Pools: Swimmer and Worker Exposure. *Environ. Sci. Technol.* **2011**, *45*, 5783−5790.
(9) Müller, S. R.; Zweifel, H.-R.; Kinnison, D. J.; Jacobsen, J. A.; Meier, M. A.; Ulrich, M. M.; Schwarzenbach, R. P. Occurrence, Sources, and Fate of Trichloroacetic Acid in Swiss Waters. *Environ. Toxicol. Chem.* **1996**, *15*, 1470−1478.
(10) Reimann, S.; Grob, K.; Frank, H. Chloroacetic Acids in Rainwater. *Environ. Sci. Technol.* **1996**, *30*, 2340−2344.
(11) Scott, B. F.; MacTavish, D.; Spencer, C.; Strachan, W. M. J.; Muir, D. C. G. Haloacetic Acids in Canadian Lake Waters and Precipitation. *Environ. Sci. Technol.* **2000**, *34*, 4266−4272.
(12) Sims, J. L.; Suflita, J. M.; Russell, H. H. *Reductive Dehalogenation of Organic Contaminants in Soils and Ground Water*; United States Environmental Protection Agency, Office of Research and Development, Office of Solid Waste and Emergency Response: Superfund Technology Support Center for Ground Water, Robert S. Kerr Environmental Research Laboratory, 1991.
(13) Seech, A. G.; Cairns, J. E.; Marvan, I. J. Method for Dehalogenation and Degradation of Halogenated Organic Contaminants. *Google Patents*, US 5,411,664 A, 2 May 1995.
(14) Mcnab, W. W.; Ruiz, R.; Reinhard, M. In-Situ Destruction of Chlorinated Hydrocarbons in Groundwater Using Catalytic Reductive Dehalogenation in a Reactive Well: Testing and Operational Experiences. *Environ. Sci. Technol.* **2000**, *34*, 149−153.
(15) Birke, V.; Mattik, J.; Runne, D. Mechanochemical Reductive Dehalogenation of Hazardous Polyhalogenated Contaminants. *J. Mater. Sci.* **2004**, *39*, 5111−5116.
(16) Esclapez, M. D.; Sáez, V.; Milán-Yáñez, D.; Tudela, I.; Louisnard, O.; González-García, J. Sonoelectrochemical Treatment of Water Polluted with Trichloroacetic Acid: From Sonovoltammetry to Pre-Pilot Plant Scale. *Ultrason. Sonochem.* **2010**, *17*, 1010−1020.
(17) Cermenati, L.; Albini, A.; Pichat, P.; Guillard, C. TiO_2 Photocatalytic Degradation of Haloquinolines in Water: Aromatic Products GM-MS Identification. Role of Electron Transfer and Superoxide. *Res. Chem. Intermed.* **2000**, *26*, 221−234.
(18) Lifongo, L. L.; Bowden, D. J.; Brimblecombe, P. Photodegradation of Haloacetic Acids in Water. *Chemosphere* **2004**, *55*, 467−476.
(19) Bosma, T.; Damborský, J.; Stucki, G.; Janssen, D. B. Biodegradation of 1, 2, 3-Trichloropropane through Directed Evolution and Heterologous Expression of a Haloalkane Dehalogenase Gene. *Appl. Environ. Microbiol.* **2002**, *68*, 3582−3587.
(20) Behbahani, M.; Lin, B.; Phares, T. L.; Seo, Y. Understanding the Impact of Water Distribution System Conditions on the Biodegradation of Haloacetic Acids and Expression of Bacterial Dehalogenase Genes. *J. Hazard. Mater.* **2018**, *351*, 293−300.
(21) Kastanek, F.; Maleterova, Y.; Kastanek, P. Combination of Advanced Oxidation and/or Reductive Dehalogenation and Biodegradation for the Decontamination of Waters Contaminated with Chlorinated Organic Compounds. *Sep. Sci. Technol.* **2007**, *42*, 1613−1625.
(22) Altamar, L.; Fernández, L.; Borras, C.; Mostany, J.; Carrero, H.; Scharifker, B. Electroreduction of Chloroacetic Acids (Mono-, Di- and Tri-) at PolyNi(II)-Tetrasulfonated Phthalocyanine Gold Modified Electrode. *Sens. Actuators, B* **2010**, *146*, 103−110.
(23) Jin, M.; Ma, H. Electrochemical Reductive Dechlorination of Trichloroacetic Acid on Porous Ag-Pd Thin Foam. *Russ. J. Electrochem.* **2013**, *49*, 1081−1085.
(24) Lei, C.; Liang, F.; Li, J.; Chen, W.; Huang, B. Electrochemical Reductive Dechlorination of Chlorinated Volatile Organic Compounds (Cl-VOCs): Effects of Molecular Structure on the Dehalogenation Reactivity and Mechanisms. *Chem. Eng. J.* **2019**, *358*, 1054−1064.
(25) Mao, R.; Lan, H.; Yan, L.; Zhao, X.; Liu, H.; Qu, J. Enhanced Indirect Atomic H* Reduction at a Hybrid Pd/Graphene Cathode for Electrochemical Dechlorination under Low Negative Potentials. *Environ. Sci.: Nano* **2018**, *5*, 2282−2292.
(26) Mao, R.; Li, N.; Lan, H.; Zhao, X.; Liu, H.; Qu, J.; Sun, M. Dechlorination of Trichloroacetic Acid Using a Noble Metal-Free Graphene−Cu Foam Electrode via Direct Cathodic Reduction and Atomic H. *Environ. Sci. Technol.* **2016**, *50*, 3829−3837.
(27) Ordaz, A. A.; Rocha, J. M.; Aguilar, F. J. A.; Granados, S. G.; Bedioui, F. Electrocatalysis of the Reduction of Organic Halide Derivatives at Modified Electrodes Coated by Cobalt and Iron Macrocyclic Complex-Based Films: Application to the Electrochemical Determination of Pollutants. *Analusis* **2000**, *28*, 238−244.
(28) Drennan, D. M.; Koshy, R. E.; Gent, D. B.; Schaefer, C. E. Electrochemical Treatment for Greywater Reuse: Effects of Cell Configuration on COD Reduction and Disinfection Byproduct Formation and Removal. *Water Supply* **2019**, *19*, 891−898.
(29) Esclapez, M. D.; Díez-García, M. I.; Sáez, V.; Bonete, P.; González-García, J. Electrochemical Degradation of Trichloroacetic Acid in Aqueous Media: Influence of the Electrode Material. *Environ. Technol.* **2013**, *34*, 383−393.
(30) *PA:NMX Palladium*; https://www.nasdaq.com/market-activity/commodities/pa%3Anmx.
(31) Chaplin, B. P. The Prospect of Electrochemical Technologies Advancing Worldwide Water Treatment. *Acc. Chem. Res.* **2019**, *52*, 596−604.
(32) Almassi, S.; Li, Z.; Xu, W.; Pu, C.; Zeng, T.; Chaplin, B. P. Simultaneous Adsorption and Electrochemical Reduction of N-Nitrosodimethylamine Using Carbon-Ti_4O_7 Composite Reactive Electrochemical Membranes. *Environ. Sci. Technol.* **2019**, *53*, 928−937.
(33) Gayen, P.; Chen, C.; Abiade, J. T.; Chaplin, B. P. Electrochemical Oxidation of Atrazine and Clothianidin on Bi-Doped SnO_2-Ti_nO_{2n-1} Electrocatalytic Reactive Electrochemical Membranes. *Environ. Sci. Technol.* **2018**, *52*, 12675−12684.
(34) Gayen, P.; Spataro, J.; Avasarala, S.; Ali, A.-M.; Cerrato, J. M.; Chaplin, B. P. Electrocatalytic Reduction of Nitrate Using Magnéli Phase TiO_2 Reactive Electrochemical Membranes Doped with Pd-Based Catalysts. *Environ. Sci. Technol.* **2018**, *52*, 9370−9379.
(35) Jing, Y.; Almassi, S.; Mehraeen, S.; LeSuer, R. J.; Chaplin, B. P. The Roles of Oxygen Vacancies, Electrolyte Composition, Lattice Structure, and Doping Density on the Electrochemical Reactivity of Magnéli Phase TiO_2 Anodes. *J. Mater. Chem. A* **2018**, *6*, 23828−23839.
(36) Nayak, S.; Chaplin, B. P. Fabrication and Characterization of Porous, Conductive, Monolithic Ti_4O_7 Electrodes. *Electrochim. Acta* **2018**, *263*, 299−310.
(37) Radjenović, J.; Farré, M. J.; Mu, Y.; Gernjak, W.; Keller, J. Reductive Electrochemical Remediation of Emerging and Regulated Disinfection Byproducts. *Water Res.* **2012**, *46*, 1705−1714.
(38) Szebényi-Győri, E.; Gagyi-Pálffy, E.; Bajnóczy, G.; Prépostffy, E. Dechlorination of Chlorinated Hydrocarbons in a Monopolar Packed Bed Electrochemical Reactor. *Period. Polytech. Chem. Eng.* **1999**, *43*, 65−76.
(39) Fang, Y.; Al-Abed, S. R. Modeling the Electrolytic Dechlorination of Trichloroethylene in a Granular Graphite-Packed Reactor. *Environ. Eng. Sci.* **2007**, *24*, 581−594.
(40) Domino, M.; Pepich, B.; Munch, D.; Fair, P.; Xie, Y. F. *EPA Method 552.3: Determination of Haloacetic Acids and Dalapon in Drinking Water by Liquidliquid Microextrcation, Derivitization and Gas Chromatography with Electron Capture Detection*. Resource Document. US EPA. 2009.
(41) Frisch, M. J.; Trucks, G. W.; Schlegel, H. B.; Scuseria, G. E.; Robb, M. A.; Cheeseman, J. R.; Scalmani, G.; Barone, V.; Petersson, G. A.; Nakatsuji, H.; Li, X.; Caricato, M.; Marenich, A. V.; Bloino, J.; Janesko, B. G.; Gomperts, R.; Mennucci, B.; Hratchian, H. P.; Ortiz, J. V.; Izmaylov, A. F.; Sonnenberg, J. L.; Williams-Young, D.; Ding, F.;

https://dx.doi.org/10.1021/acs.est.9b06744
Environ. Sci. Technol. 2020, 54, 1982−1991

Lipparini, F.; Egidi, F.; Goings, J.; Peng, B.; Petrone, A.; Henderson, T.; Ranasinghe, D.; Zakrzewski, V. G.; Gao, J.; Rega, N.; Zheng, G.; Liang, W.; Hada, M.; Ehara, M.; Toyota, K.; Fukuda, R.; Hasegawa, J.; Ishida, M.; Nakajima, T.; Honda, Y.; Kitao, O.; Nakai, H.; Vreven, T.; Throssell, K.; Montgomery, J. A., Jr.; Peralta, J. E.; Ogliaro, F.; Bearpark, M. J.; Heyd, J. J.; Brothers, E. N.; Kudin, K. N.; Staroverov, V. N.; Keith, T. A.; Kobayashi, R.; Normand, J.; Raghavachari, K.; Rendell, A. P.; Burant, J. C.; Iyengar, S. S.; Tomasi, J.; Cossi, M.; Millam, J. M.; Klene, M.; Adamo, C.; Cammi, R.; Ochterski, J. W.; Martin, R. L.; Morokuma, K.; Farkas, O.; Foresman, J. B.; Fox, D. J., *Gaussian 16*, Rev. B. *01*; Gaussian, Inc.: Wallingford, CT, 2016.

(42) Zhao, Y.; Truhlar, D. G. The M06 Suite of Density Functionals for Main Group Thermochemistry, Thermochemical Kinetics, Noncovalent Interactions, Excited States, and Transition Elements: Two New Functionals and Systematic Testing of Four M06-Class Functionals and 12 Other Functionals. *Theor. Chem. Acc.* **2008**, *120*, 215−241.

(43) Marenich, A. V.; Cramer, C. J.; Truhlar, D. G. Universal Solvation Model Based on Solute Electron Density and on a Continuum Model of the Solvent Defined by the Bulk Dielectric Constant and Atomic Surface Tensions. *J. Phys. Chem. B* **2009**, *113*, 6378−6396.

(44) Kelly, C. P.; Cramer, C. J.; Truhlar, D. G. Adding Explicit Solvent Molecules to Continuum Solvent Calculations for the Calculation of Aqueous Acid Dissociation Constants. *J. Phys. Chem. A* **2006**, *110*, 2493−2499.

(45) Tissandier, M. D.; Cowen, K. A.; Feng, W. Y.; Gundlach, E.; Cohen, M. H.; Earhart, A. D.; Coe, J. V.; Tuttle, T. R. The Proton's Absolute Aqueous Enthalpy and Gibbs Free Energy of Solvation from Cluster-Ion Solvation Data. *J. Phys. Chem. A* **1998**, *102*, 7787−7794.

(46) Bard, A. J.; Faulkner, L. R. Fundamentals and Applications. *Electrochem. Methods* **2001**, *2*, 482.

(47) Tung, H.-H.; Unz, R. F.; Xie, Y. F. HAA Removal by GAC Adsorption. *J. - Am. Water Works Assoc.* **2006**, *98*, 107−112.

(48) Desta, M. B. Batch Sorption Experiments: Langmuir and Freundlich Isotherm Studies for the Adsorption of Textile Metal Ions onto Teff Straw (Eragrostis Tef) Agricultural Waste. *J. Thermodyn.* **2013**, *2013*, 375830.

(49) Reed, B. E.; Matsumoto, M. R. Modeling Cadmium Adsorption by Activated Carbon Using the Langmuir and Freundlich Isotherm Expressions. *Sep. Sci. Technol.* **1993**, *28*, 2179−2195.

(50) Hozalski, R. M.; Zhang, L.; Arnold, W. A. Reduction of Haloacetic Acids by Fe0: Implications for Treatment and Fate. *Environ. Sci. Technol.* **2001**, *35*, 2258−2263.

(51) Liu, Y.; Mao, R.; Tong, Y.; Lan, H.; Zhang, G.; Liu, H.; Qu, J. Reductive Dechlorination of Trichloroacetic Acid (TCAA) by Electrochemical Process over Pd-In/Al_2O_3 Catalyst. *Electrochim. Acta* **2017**, *232*, 13−21.

(52) Lou, Z.; Li, Y.; Zhou, J.; Yang, K.; Liu, Y.; Baig, S. A.; Xu, X. TiC Doped Palladium/Nickel Foam Cathode for Electrocatalytic Hydrodechlorination of 2,4-DCBA: Enhanced Electrical Conductivity and Reactive Activity. *J. Hazard. Mater.* **2019**, *362*, 148−159.

(53) Yao, Q.; Zhou, X.; Xiao, S.; Chen, J.; Abdelhafeez, I. A.; Yu, Z.; Chu, H.; Zhang, Y. Amorphous Nickel Phosphide as a Noble Metal-Free Cathode for Electrochemical Dechlorination. *Water Res.* **2019**, *165*, 114930.

(54) Muller, J.; Huaux, F.; Moreau, N.; Misson, P.; Heilier, J.-F.; Delos, M.; Arras, M.; Fonseca, A.; Nagy, J. B.; Lison, D. Respiratory Toxicity of Multi-Wall Carbon Nanotubes. *Toxicol. Appl. Pharmacol.* **2005**, *207*, 221−231.

(55) Bottini, M.; Bruckner, S.; Nika, K.; Bottini, N.; Bellucci, S.; Magrini, A.; Bergamaschi, A.; Mustelin, T. Multi-Walled Carbon Nanotubes Induce T Lymphocyte Apoptosis. *Toxicol. Lett.* **2006**, *160*, 121−126.

(56) Ding, L.; Stilwell, J.; Zhang, T.; Elboudwarej, O.; Jiang, H.; Selegue, J. P.; Cooke, P. A.; Gray, J. W.; Chen, F. F. Molecular Characterization of the Cytotoxic Mechanism of Multiwall Carbon Nanotubes and Nano-Onions on Human Skin Fibroblast. *Nano Lett.* **2005**, *5*, 2448−2464.

(57) Das, R.; Leo, B. F.; Murphy, F. The Toxic Truth about Carbon Nanotubes in Water Purification: A Perspective View. *Nanoscale Res. Lett.* **2018**, *13*, 183.

(58) Korshin, G. V.; Jensen, M. D. Electrochemical Reduction of Haloacetic Acids and Exploration of Their Removal by Electrochemical Treatment. *Electrochim. Acta* **2001**, *47*, 747−751.

https://dx.doi.org/10.1021/acs.est.9b06744
Environ. Sci. Technol. 2020, 54, 1982−1991